WHY IS NON-THERMAL LINE BROADENING OF SPECTRAL LINES IN THE LOWER TRANSITION REGION OF THE SUN INDEPENDENT OF SPATIAL RESOLUTION?

B. De Pontieu[1,2], S. McIntosh[3], J. Martinez-Sykora[4,1], H. Peter[5], and T.M.D. Pereira[2]
[1]Lockheed Martin Solar & Astrophysics Lab, Org. A021S, Bldg. 252, 3251 Hanover Street Palo Alto, CA 94304, USA
[2]Institute of Theoretical Astrophysics, University of Oslo, P.O. Box 1029 Blindern, N-0315 Oslo, Norway
[3]High Altitude Observatory, National Center for Atmospheric Research, P.O. Box 3000, Boulder, CO 80307
[4]Bay Area Environmental Research Institute, Sonoma, CA 94952, USA and
[5]Max-Planck-Institut für Sonnensystemforschung, Justus-von-Liebig-Weg 3, D-37077 Göttingen, Germany
Draft version October 19, 2017

ABSTRACT

Spectral observations of the solar transition region (TR) and corona show broadening of spectral lines beyond what is expected from thermal and instrumental broadening. The remaining non-thermal broadening is significant (5-30 km/s) and correlated with the intensity. Here we study spectra of the TR Si IV 1403 Å line obtained at high resolution with the Interface Region Imaging Spectrograph (IRIS). We find that the large improvement in spatial resolution ($0.33''$) of IRIS compared to previous spectrographs ($2''$) does not resolve the non-thermal line broadening which in most regions remains at pre-IRIS levels of about 20 km/s. This invariance to spatial resolution indicates that the processes behind the broadening occur along the line-of-sight (LOS) and/or on spatial scales (perpendicular to the LOS) smaller than 250 km. Both effects appear to play a role. Comparison with IRIS chromospheric observations shows that, in regions where the LOS is more parallel to the field, magneto-acoustic shocks driven from below impact the TR and can lead to significant non-thermal line broadening. This scenario is supported by MHD simulations. While these do not show enough non-thermal line broadening, they do reproduce the long-known puzzling correlation between non-thermal line broadening and intensity. This correlation is caused by the shocks, but only if non-equilibrium ionization is taken into account. In regions where the LOS is more perpendicular to the field, the prevalence of small-scale twist is likely to play a significant role in explaining the invariance and correlation with intensity.

Keywords: waves - Sun:atmospheric motions - Sun:magnetic fields - Sun: chromosphere - Sun:transition region - Sun:corona

1. INTRODUCTION

The transition region between the chromosphere and corona has long puzzled solar physicists (see Mariska 1992, and references therein). Spectroscopic observations of the first three moments of TR spectral lines have presented difficult challenges to observers and theorists alike. For example, low-resolution intensity measurements of TR lines have been difficult to reproduce in coronal heating models leading to a debate about the TR magnetic topology and the role of unresolved fine structure (UFS) which recent IRIS observations may have finally resolved (Hansteen et al. 2014). Similarly, low-resolution observations of TR velocities have revealed a pervasive redshift (Peter & Judge 1999; Peter 1999) that is thought be a signature of the dominant heating mechanism in the corona and which remains the subject of vigorous debate (Peter et al. 2004; Hansteen et al. 2010). Finally, the non-thermal line broadening of TR lines has been interpreted as a signature of a variety of physical processes such as small-scale flows, coronal nanoflares, Alfvén waves, turbulence, etc. (Mariska 1992). One potentially important clue to the nature of non-thermal broadening is the puzzling and unexplained correlation between the intensity and non-thermal line broadening of low TR lines (see, e.g., Erdelyi et al. 1998; Chae et al. 1998).

One major issue that has hampered progress in our understanding of the TR is that it has often been observed at inadequate spatial, temporal and spectral resolution, or in isolation from the regions that impact its dynamics such as the chromosphere and corona. The advent of IRIS (De Pontieu et al. 2014b) for the first time provides spectra and images of the TR at high spatial ($0.33''$), temporal ($\sim 2s$) and spectral (3 km/s) resolution, all of which are significant improvements over previous instrumentation such as SUMER with resolutions of respectively, $2''$, 10s and 8 km/s (Wilhelm et al. 1995). In addition, IRIS provides chromospheric spectra and images in the strong Mg II h spectral line at the same time and location as the TR spectra.

In this paper we focus on high-resolution observations of the Si IV 1402.7Å spectral line in active regions (AR), quiet Sun (QS) and coronal hole (CH). We provide an overview of the datasets used in §2. In §3 we describe how non-thermal line broadening and its correlation with intensity is invariant to spatial and temporal summing, and how some of the increased line broadening appears to be caused by chromospheric shocks. We compare our observations with advanced numerical simulations that include the effects of non-equilibrium ionization in the TR in §4. We finish with a discussion of the impact of our results in §5.

2. DATASETS

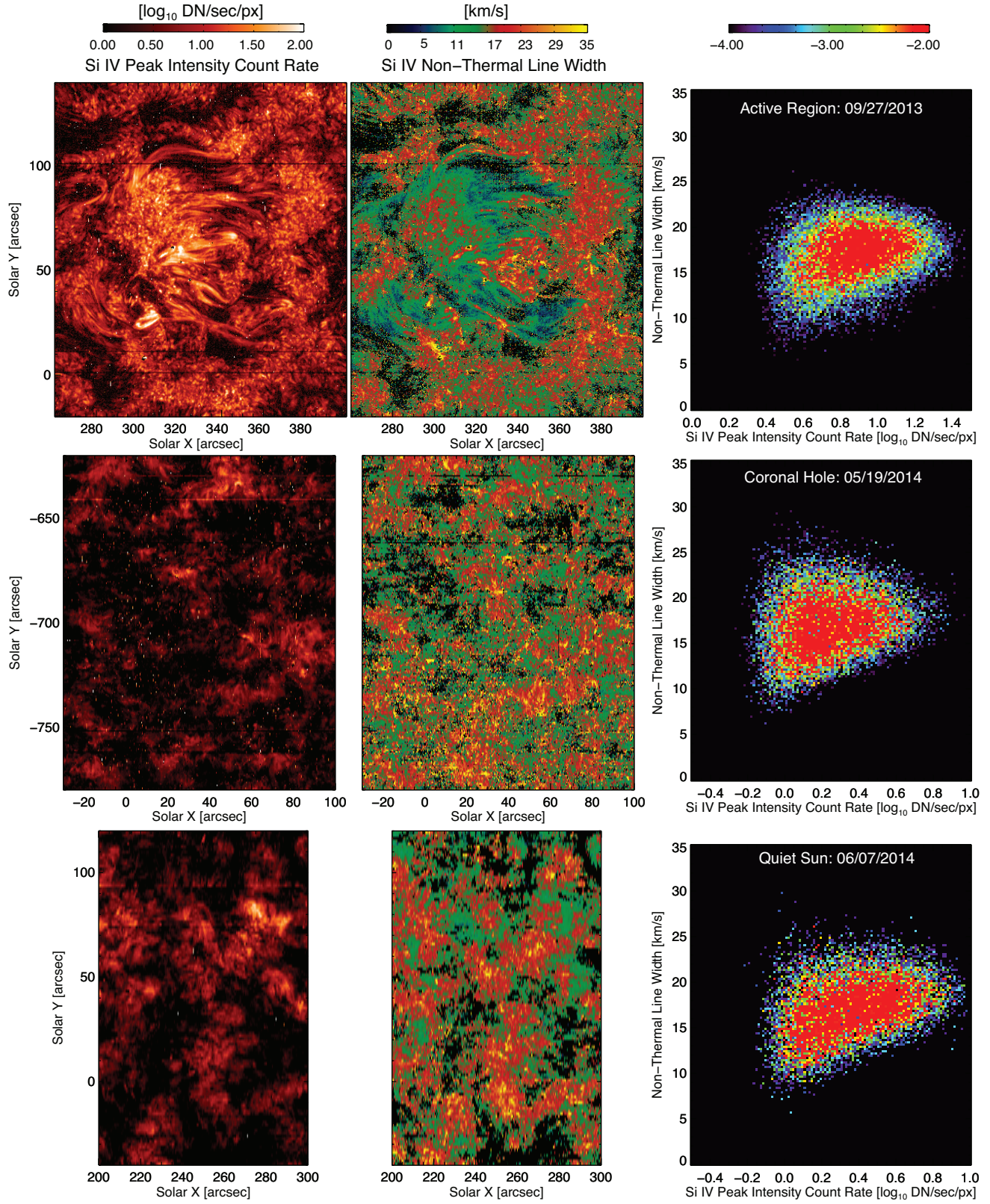We use several different IRIS datasets: three raster scans and two sit-and-stare sequences. The raster scans

Figure 1. Comparison of S IV 1403Å peak line intensity and non-thermal widths for three different solar domains in rows from top to bottom: active region, coronal hole, and quiet Sun for a single Gaussian fit to the observed IRIS line profiles. The left column of panels show the spatial variation of the ($\log_{10}$) peak line intensity, while the central column shows the corresponding non-thermal line width and the right column shows the two-dimensional histogram of the former quantities.

were taken on 2013-Sep-27 for AR, 2014-June-7 for QS and 2013-May-19 for CH. The sit-and-stare sequences (including solar rotation compensation) were both taken on 2013-Sep-10 with the AR sequence starting at 08:09

UT and the CH sequence starting at 23:09 UT. All of the IRIS data were calibrated to level 2, i.e., including dark current, flat-field and geometric correction, as well as co-alignment between various channels. We also corrected for the spectral drift associated with the spacecraft's orbital velocity and the drift caused by thermal variations during one orbit. The slit-jaw images (SJI) were corrected for dark-current and flat-field, as well as internal co-alignment drifts (De Pontieu et al. 2014b). We perform single Gaussian fits to spectral line profiles in locations with sufficient signal-to-noise. From the fits we determine the peak intensity I_p, the Doppler shift v_D and the 1/e line width σ. The latter is used to determine the non-thermal line broadening σ_{nt} with $\sigma_{nt} = \sqrt{\sigma^2 - \sigma_{th}^2 - \sigma_{inst}}$ where $\sigma_{th} = 6.86$ km/s (assuming a formation temperature of 80,000 K, see also McIntosh et al. 2008) and $\sigma_{inst} = 3.9$ km/s (De Pontieu et al. 2014b).

3. OBSERVATIONS

IRIS observations of Si IV in AR, QS and CH show a variety of bright features that include footpoints of loops (plage in AR, network in QS) or the solar wind (network in CH) as well as less bright regions, typically away from the strong flux concentrations that underlie the bright network/plage regions. Comparison of the left panels with the middle panels of Fig. 1 shows that the non-thermal line broadening is often enhanced in the brightest regions. This correlation is not perfect on a pixel-to-pixel basis, but clearly exists on larger scales. This is confirmed by the right panels of Fig. 1 which show how the non-thermal line broadening is correlated with the logarithm of the peak intensity of the line. This correlation was previously found using spectra from lower resolution instruments (Mariska 1992), but our observations show that it does not change character at the very high spatial and temporal resolution of IRIS.

Surprisingly, we find that the non-thermal line broadening is of order 20 km/s, even at the very high spatial resolution of $0.16''$(pixel size) by $0.33''$(slit width) that IRIS provides. More surprising is that the average non-thermal line broadening observed with IRIS for AR, QS and CH are similar in value to measurements with lower resolution instruments (e.g. Chae et al. 1998). This is confirmed when we spatially rebin our observations to superpixels that are 2x2 original IRIS pixels and once again perform a single Gaussian fit to the spectra. The resulting histogram of non-thermal line broadening is essentially identical to the histogram at IRIS native resolution (Fig. 2). This invariance to spatial summing occurs at 4x4 and 8x8 spatial resolution as well, as shown in Fig. 2. A similar invariance occurs for temporal summing.

At first sight it may seem surprising that the significant increase in spatial resolution of IRIS does not lead to reduced non-thermal line broadening, since a map of Doppler shifts indicates that there is a significant variation of the line-of-sight velocity on subarcsecond spatial scales (not shown). However, the variation in line-of-sight velocities (or macro-turbulence) on arcsecond scales is clearly not large enough to cause significant additional broadening. Instead, the invariance to spatial and temporal summing indicates that the processes responsible for the non-thermal line broadening either occur on spatial scales that are smaller than the native IRIS resolution ($0.16''$x $0.33''$) and/or occur along the line-of-sight (since Si IV 1402.7Å is optically thin).

What are these processes, and can we find evidence for them in our data? First, De Pontieu et al. (2014a) report on how the chromosphere and TR are replete with twisting motions on spatial scales down to the IRIS resolution. Their findings and previous results indicate that twist occurs on a variety of spatial scales, from macrospicules and tornadoes down to the 0.33 arcsec scales IRIS can observe, and that this distribution of twist extends also to scales that are smaller than IRIS can resolve. De Pontieu et al. (2014a) associate this twist with propagating Alfvén waves with amplitudes of order 10-30 km/s and illustrate how it becomes most easily visible when the line-of-sight is more perpendicular to the direction of the magnetic field. In our data we find support for such a scenario with many of the apparently low-lying loops that connect the two plage regions in Fig. 1 showing enhanced non-thermal line broadening. It is clear that significant non-thermal line broadening would occur because of twist that is part of the same distribution as De Pontieu et al. (2014a) report but on smaller scales than IRIS can observe.

However, here we focus on another mechanism that has been overlooked and appears to act when the line-of-sight is more parallel to the magnetic field. In locations of increased line broadening in plage/network regions, i.e., where the magnetic field is typically more vertical, we find a correlation between increased line broadening and the passage of magneto-acoustic shocks driven from the chromosphere (Fig. 3). These shocks are typically upward propagating and have previously been reported as being ubiquitous in the magnetic chromosphere (e.g. Hansteen et al. 2006; De Pontieu et al. 2007; Rouppe van der Voort et al. 2007; Langangen et al. 2008b,a; Vecchio et al. 2009). The formation of these shocks is thought to be caused by several mechanisms, e.g., leakage of photospheric waves, convective motions or magnetic energy release in the photosphere (e.g. Heggland et al. 2007; Martínez-Sykora et al. 2009; Heggland et al. 2011). The subsequent upward propagation along a guiding magnetic field leads to slow-mode magneto-acoustic shocks in a low plasma β environment. The shocks are recognizable as saw-tooth patterns in so-called $\lambda - t$ (wavelength-time) plots of the Mg II h line (Fig. 3). The saw-tooth patterns show how the h3 spectral feature repeatedly swings abruptly from the red wing to the blue wing of the Mg II h line as the shock propagates through the line formation region of the h3 feature (i.e., the top of the chromosphere, Leenaarts et al. 2013a,b; Pereira et al. 2013). Figure 3 shows that these chromospheric shocks have a variable impact on the Si IV spectral line profiles. Sometimes the shock signal is clearly visible in the TR line as a rapid brightness excursion to the blue followed by a linear shift with time to the red (e.g., panel B of Fig. 3 around t=700-900s). At other times a shock signal is present in the TR, but at much lower intensities (e.g., t=2100 s in panel B of Fig. 3). However, it is clear that in a plage region (Fig. 3a,b) the rapid excursions to the blue at the time of a Mg II h shock (Fig. 3a) are often brightest in Si IV. In addition, the line width from a single Gaussian fit to Si IV 1402.7Å (white or red symbols,
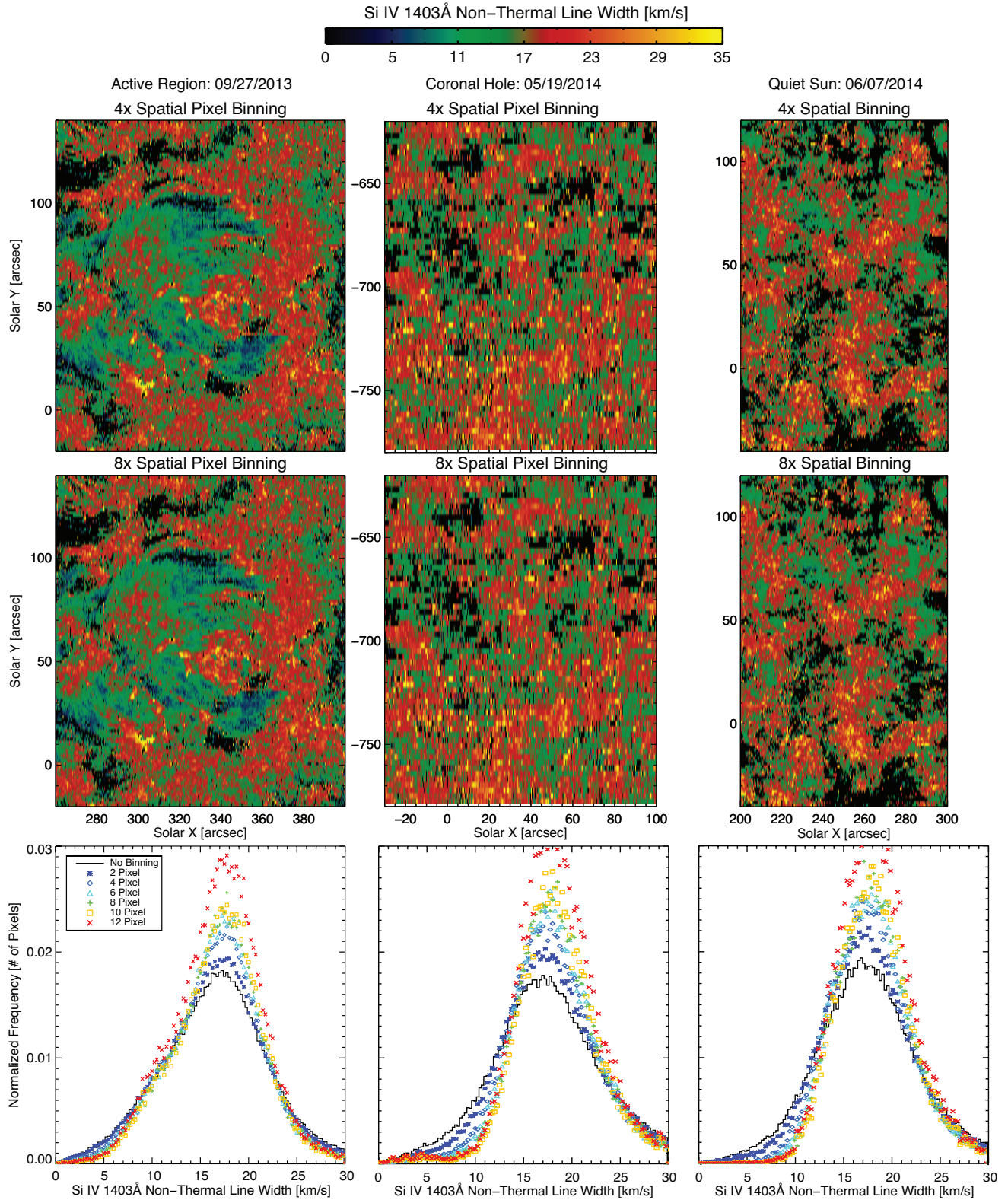
Figure 2. Variations of the active region (left), coronal hole (center) and quiet sun (right) Si IV 1403Å non-thermal line widths when different levels of spatial binning are applied to the Si IV line spectra prior to fitting with a single Gaussian profile (cf. the central panels of Fig. 1). The top row of panels shows the non-thermal line width when four spatial pixels are co-added in each case while the central row shows the same quantities with eight spatial pixels co-added. The bottom row of panels shows the variation of the non-thermal line width at a range of spatial bindings from the native resolution of the instrument to twelve pixels as indicated in the panel legend (bottom left).

Fig. 3a) often significantly increases when the shock passage leads to a very rapid switch from red to blueshifts, e.g., at $t = 200, 700, 1050, 1550, 2700$ s. This suggests that the increased non-thermal line broadening in these
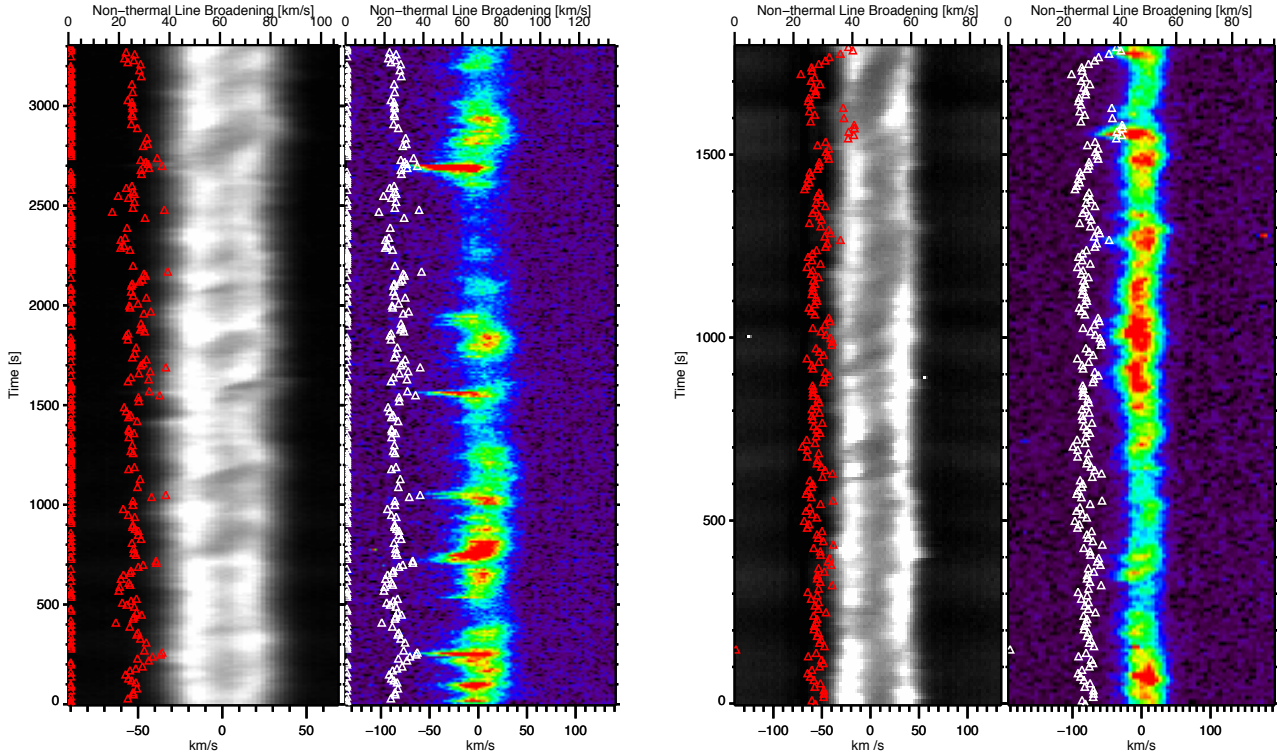
Figure 3. Wavelength vs. time (λ-t) plots for locations in plage (a, b) and a network region in a coronal hole (c, d) for the Mg II h 2803Å line (a, c) and the Si IV 1402.7Å line (b, d). Overplotted in red and white is the evolution of the non-thermal line broadening as derived from a single Gaussian fit to the Si IV line. The non-thermal line broadening scale is shown on the top axis. The non-thermal line broadening is set to 0 for profiles in which the signal is too weak and/or the single Gaussian fit is poor. Notice the correlation between shock occurrence (swing from red to blue) in the Mg II h line and the increased line broadening and brightness in Si IV.

locations may be caused by the large range of velocities in the pre- and post-shock environment, both of which are covered by the line formation region. An alternative interpretation would be turbulence caused by the shock passage, although it is unclear why the increased broadening would occur when the switch from red to blueshifts happens.

The former scenario seems to hold for the CH network region although the lack of a strong guiding magnetic field (compared to plage) leads to a less clear one-to-one correlation between shock signatures in Mg II h and Si IV. The magnetic field in coronal holes is less strong and not as vertical as in plage, which can easily lead to slight spatial displacements between the chromospheric shock and the TR counterpart. Nevertheless, there is still a correlation between strong chromospheric velocity excursions and brightenings and associated non-thermal line broadening in the TR.

Clearly, the influence of magneto-acoustic shocks and their impact on non-thermal line broadening could provide a straightforward explanation for the observed invariance to spatio-temporal summing of the broadening. It could also explain why there is a correlation between non-thermal broadening and the intensity, with shock heating causing strong brightening, as well as non-thermal line broadening.

We note that the non-thermal line broadening is also increased during times when Mg II h is not switching from strong red- to blueshifts.

4. NUMERICAL SIMULATIONS

While these observations provide a possible reason for the observed invariance and correlations, they are also puzzling. In particular, one would not expect the line formation region of Si IV 1402.7Å to cover both the pre- and post-shock environment given that under ionization equilibrium conditions the line is expected to from mostly in a narrow temperature range around $80,000\pm20,000$K. Numerical simulations of a computational domain ranging from the top of the convection zone into the corona help shed light on this. We performed a 2.5D radiative MHD simulation using the Bifrost code (Gudiksen et al. 2011) in which the main free parameter is the magnetic field configuration. Bifrost includes thermal conduction and optically thin radiative losses in the corona, as well as radiative losses in the optically thick chromosphere and photosphere. The initial field configuration was chosen to be representative of a coronal hole (average unsigned flux of 5 Mx cm^{-2}). We calculated the Si ionization in two different ways: 1. ionization equilibrium, 2. non-equilibrium, i.e., time-dependent, ionization of Si (using the approach of Olluri et al. 2013). We calculate Si IV 1402.7Å emission using CHIANTI (Landi et al. 2012) and optically thick Mg II h 2803Å spectral line profiles using RH 1.5D (Pereira & Uitenbroek 2014).

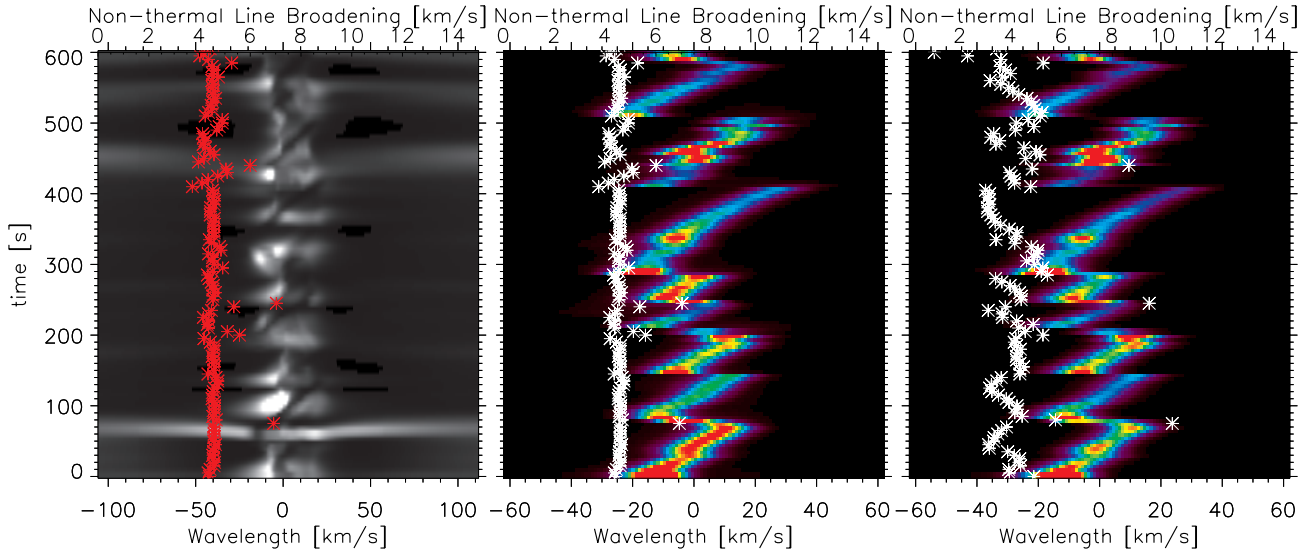We find that both results show evidence of magneto-

Figure 4. λ t plots for the Mg II h 2803Å line (a) and the Si IV 1402.7Å line (b, c) from numerical simulations of a unipolar environment assuming ionization equilibrium (a, b) and non-equilibrium ionization for Si^{3+} (c). Overplotted in red or white are the evolution of the non-thermal line broadening as derived from a single Gaussian fit to the Si IV line. Notice the correlation between shock occurrence (swing from red to blue) in the Mg II h line and the increased line broadening and brightness in Si IV.

acoustic shocks that propagate from the chromosphere into the TR. As shown in Fig. 4 the simulated shocks lead to increased non-thermal line broadening in the TR at the time of the shock passage. However, this is more evident in the simulation assuming non-equilibrium ionization: the broadening is increased by 2-10 km/s during shock passage, and by several km/s throughout the simulation. More importantly, the ionization equilibrium simulation does not reproduce the correlation (Fig. 5) between non-thermal line broadening and the logarithm of the intensity. That correlation only appears when non-equilibrium ionization is included in the simulations, as shown in Fig. 5.

This is because the non-equilibrium ionization leads to the presence of Si^{3+} ions over a much wider range of temperatures than under ionization equilibrium (see, e.g. Olluri et al. 2013): many locations show Si^{3+} ionization fractions above 20% over a temperature range from $10,000$ to $200,000$ K, with most of the Si IV emission resulting from plasma at temperatures between 20,000 and 200,000 K. This means that the line formation region more easily captures both the pre- and post-shock environment. This naturally leads to a larger range of velocities along the line-of-sight of the optically thin Si IV lines, and thus non-thermal line broadening. This sensitivity to the shocks provides a natural explanation for the correlation between intensity and non-thermal line broadening.

The models are numerical experiments. While they reproduce aspects of our observations, they are currently unable to reproduce the large non-thermal line broadening that is observed. This is likely because the numerical resistivity leads to energy deposition on larger spatial scales than in the solar atmosphere, leading to less violent shocks and other events.

5. DISCUSSION & CONCLUSION

Our IRIS observations and numerical simulations suggest that the observed invariance to spatio-temporal res-
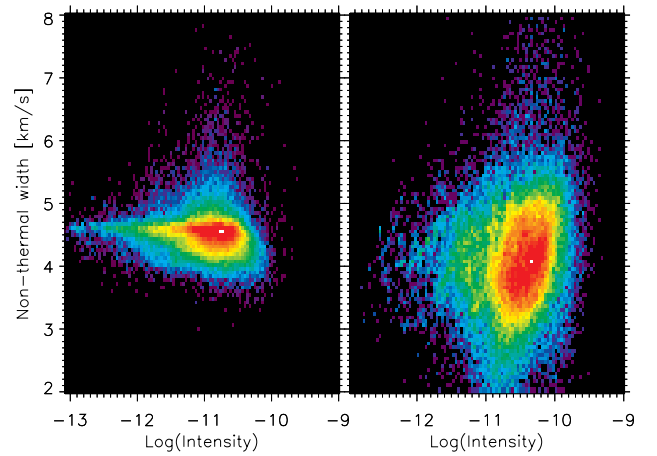

Figure 5. Probability density function between logarithm of the Si IV 1402.7Å intensity and its non-thermal line broadening, for simulations with ionization equilibrium (left) and including non-equilibrium ionization (right). Note the lack of correlation in the ionization equilibrium simulations, and the appearance of a correlation for non-equilibrium ionization.

olution of the non-thermal line broadening of Si IV 1402.Å, and its correlation with the intensity may have two causes. First, in regions where the line-of-sight is more perpendicular to the local magnetic field the presence of twisting motions or other turbulent motions on sub-resolution scales likely plays a role in both effects. We find direct evidence that in regions where the line-of-sight is more parallel with the magnetic field (e.g., network or plage regions) the presence of magneto-acoustic shocks along the line-of-sight can lead to enhanced non-thermal line broadening, as well as its correlation with the intensity. This sheds some doubt on previous studies which have emphasized or hypothesized about how the correlation between intensity and non-thermal broadening is indicative of or gives clues about the coronal heating mechanism (nanoflares) or turbulence. Our results suggest that this may not be the case and that

instead the tight connection between chromospheric and TR dynamics plays an important role in the observed line broadening in the TR.

The correlation with slow-mode magneto-acoustic shock waves also provides a natural explanation for why correlations between parameters of TR lines with increasing temperature differences become worse. The effects of the shocks at high temperatures are diminished as thermal conduction starts to smooth out the strong gradients associated with shocks.

The center-to-limb variation of the non-thermal line width is small, if present at all (Peter & Judge 1999). While the effect of the shocks (mostly $\|B$) should decrease towards the limb, the effect of the twisting motions (mostly $\perp B$) should increase towards the limb. How these two effects combine to lead to a roughly constant center-to-limb variation remains to be investigated in detail, but is likely similar to the results of McIntosh et al. (2008) who investigated the trade-off between field-aligned shock-driven jets and transverse wave motions of the same size.

Our comparison of the observations with numerical modeling suggests that non-equilibrium ionization may play an important role in the diagnostics, dynamics and energetics of the TR, as already suggested by advanced simulations (Olluri et al. 2013). The fact that non-equilibrium ionization leads to TR emission that originates over a larger temperature/height range, implies that, in the presence of shocks with strong velocity gradients, some of the non-thermal line broadening observed is caused by relatively mundane slow-mode magneto-acoustic shocks. Such shocks are plentiful in the chromosphere and it would be very surprising if they did not affect the TR in some fashion. Other effects that impact the chromosphere/transition region, such as ambipolar diffusion caused by the interactions between ions and neutrals, may also play a role in these types of diagnostics.

Several unresolved issues remain. While shocks clearly play a role in causing non-thermal line broadening, especially at the time of impact of the shock in the TR, the non-thermal line broadening is significant even at times when the chromospheric velocity does not rapidly shift from red to blueshifts. Perhaps the increased non-thermal line broadening at other times is caused by the strong velocity gradients in the pre-shock or post-shock plasma combined with non-equilibrium ionization and other effects that lead to TR emission over a wide range of heights? Alternatively, the simulations do not contain type 2 spicules which, based on their observational characteristics, likely show strong flows and strong gradients and could thus also contribute to non-thermal line broadening.

It also remains unclear how the pervasive redshifts in the TR fit into the picture we have sketched in the above. Further numerical and observational studies will be required to settle that issue.

REFERENCES

Chae, J., Schühle, U., & Lemaire, P. 1998, ApJ, 505, 957

De Pontieu, B., Hansteen, V. H., Rouppe van der Voort, L., van Noort, M., & Carlsson, M. 2007, ApJ, 655, 624

De Pontieu, B., Rouppe van der Voort, L., McIntosh, S. W., et al. 2014a, Science, 346, D315

De Pontieu, B., Title, A. M., Lemen, J. R., et al. 2014b, Sol. Phys., 289, 2733

Erdelyi, R., Doyle, J. G., Perez, M. E., & Wilhelm, K. 1998, A&A, 337, 287

Gudiksen, B. V., Carlsson, M., Hansteen, V. H., et al. 2011, A&A, 531, A154

Hansteen, V. H., De Pontieu, B., Carlsson, M., & Lemen, J. 2014, Science, 1, 1

Hansteen, V. H., De Pontieu, B., Rouppe van der Voort, L., van Noort, M., & Carlsson, M. 2006, ApJ, 647, L73

Hansteen, V. H., Hara, H., De Pontieu, B., & Carlsson, M. 2010, ApJ, 718, 1070

Heggland, L., De Pontieu, B., & Hansteen, V. H. 2007, ApJ, 666, 1277

Heggland, L., Hansteen, V. H., De Pontieu, B., & Carlsson, M. 2011, ApJ, 743, 142

Landi, E., Del Zanna, G., Young, P. R., Dere, K. P., & Mason, H. E. 2012, ApJ, 744, 99

Langangen, Ø., Carlsson, M., Rouppe van der Voort, L., Hansteen, V., & De Pontieu, B. 2008a, ApJ, 673, 1194

Langangen, Ø., Rouppe van der Voort, L., & Lin, Y. 2008b, ApJ, 673, 1201

Leenaarts, J., Pereira, T. M. D., Carlsson, M., Uitenbroek, H., & De Pontieu, B. 2013a, ApJ, 772, 89

Leenaarts, J., Pereira, T. M. D., Carlsson, M., Uitenbroek, H., & De Pontieu, B. 2013b, ApJ, 772, 90

Mariska, J. T. 1992, The solar transition region

Martínez-Sykora, J., Hansteen, V., De Pontieu, B., & Carlsson, M. 2009, ApJ, 701, 1569

McIntosh, S. W., De Pontieu, B., & Tarbell, T. D. 2008, ApJ, 673, L219

Olluri, K., Gudiksen, B. V., & Hansteen, V. H. 2013, ApJ, 767, 43

Pereira, T. M. D., Leenaarts, J., De Pontieu, B., Carlsson, M., & Uitenbroek, H. 2013, ApJ, 778, 143

Pereira, T. M. D. & Uitenbroek, H. 2014, ArXiv e-prints

Peter, H. 1999, ApJ, 516, 490

Peter, H., Gudiksen, B. V., & Nordlund, Å. 2004, ApJ, 617, L85

Peter, H. & Judge, P. G. 1999, ApJ, 522, 1148

Rouppe van der Voort, L. H. M., De Pontieu, B., Hansteen, V. H., Carlsson, M., & van Noort, M. 2007, ApJ, 660, L169

Vecchio, A., Cauzzi, G., & Reardon, K. P. 2009, A&A, 494, 269

Wilhelm, K., Curdt, W., Marsch, E., et al. 1995, Sol. Phys., 162, 189